Clinical Cancer Research

Synergistic Killing Effect between Vorinostat and Target of CD146 in Malignant Cells

Xiaoli Ma[1,2], Jia Liu[1], Jiang Wu[1], Xiyun Yan[3], Peng Wu[1], Yong Liu[1], Shuang Li[1], Yuan Tian[1], Yang Cao[1], Gang Chen[1], Li Meng[1], Gang Xu[1], Shixuan Wang[1], Yunping Lu[1], Ding Ma[1], and Jianfeng Zhou[1]

Abstract

Purpose: Although histone deacetylase inhibitors (HDACi) are emerging as a new class of anticancer agents, one of the most significant concerns is that interactions with a wide array of substrates using these agents might initiate both therapeutic and undesired protective responses. Here, we sought to identify the potential protective reactions initiated by HDACi and determine whether targeting these reactions would enhance the antitumoral activity of HDACi.

Experimental Design: Gene expression profiles were analyzed by cDNA microarray in Molt-4 cells before and after treatment of vorinostat. Induction of CD146 by vorinostat was examined in a wide range of tumors and nonmalignant cells. AA98, an anti-CD146 monoclonal antibody, was used to target CD146 function. Synergistic antitumoral and antiangiogenic effects between AA98 and vorinostat were examined both *in vitro* and *in vivo*. The potential effect of combined AA98 and vorinostat treatment on the AKT pathway was determined by Western blotting.

Results: The induction of CD146 is a common phenomenon in vorinostat-treated cancer but not in nonmalignant cells. Targeting of CD146 with AA98 substantially enhanced vorinostat-induced killing via the suppression of activation of AKT pathways in cancer cells. Moreover, AA98 in combination with vorinostat significantly inhibited angiogenesis. *In vivo*, AA98 synergized with vorinostat to inhibit tumor growth and metastasis.

Conclusion: The present study provided the first evidence that an undesired induction of CD146 could serve as a protective response to offset the antitumor efficacy of vorinostat. On the other hand, targeting CD146 in combination with vorinostat could be exploited as a novel strategy to more effectively kill cancer cells. *Clin Cancer Res; 16(21); 5165–76. ©2010 AACR.*

Histone deacetylase inhibitors (HDACi) show promise as a novel class of anticancer agents in a wide spectrum of tumors. At least 14 HDACi are being tested in over 100 clinical trials and have displayed encouraging therapeutic responses with surprisingly good safety profiles (1, 2). The clinical potential of HDACi has been well documented by the successful development of vorinostat (suberoylanilide hydroxamic acid), which has recently been approved by the U.S. Food and Drug Administration for treating cutaneous T-cell lymphoma (3). Despite the rapid clinical progress achieved, the mechanisms of action of HDACi are not yet well understood. Early studies using gene profiling techniques have revealed that up to 17% of all known genes are affected by HDACi at the transcriptional level (4). A large number of proapoptotic or antiapoptotic genes and cell cycle regulatory genes have been independently identified by different groups as the downstream targets of HDACi. One of the central problems with respect to the action of HDACi is that modulation of such extensive substrates using these agents might result in the initiation of both therapeutic responses and undesired protective programs, which significantly limits the optimal application of this class of drugs. Identification of the potential protective reactions initiated by HDACi would be helpful in the development of more effective protocols, to identify potentially resistant patients, and facilitate the development of novel HDACi.

Recently, clinical data has shown that there is limited efficacy for HDACi as a single agent. For example, patients with myelodysplasia or acute myeloid leukemia (AML) responded to HDACi therapy; however, true partial responses or complete remissions were infrequent. Two phase I studies reported that no complete remissions or

Authors' Affiliations: [1]Cancer Biology Research Center, Tongji Hospital, Tongji Medical College, Huazhong University of Science and Technology, Wuhan, Hubei, P.R. China; [2]Beijing Obstetrics and Gynecology Hospital, Capital Medical University; and [3]Center of Molecular Biology, Institute of Biophysics, Chinese Academy of Sciences, Beijing, P.R. China

Note: Supplementary data for this article are available at Clinical Cancer Research Online (http://clincancerres.aacrjournals.org/).

X. Ma and J. Liu contributed equally to this work.

Corresponding Authors: Ding Ma or Jianfeng Zhou, Cancer Biology Research Center, Tongji Hospital, Tongji Medical College, Huazhong University of Science and Technology, 1095 Jiefang Avenue, Wuhan, Hubei 430030, P.R. China. Phone: 86-27-8366-3351; Fax: 86-27-8366-2681; E-mail: dma@tjh.tjmu.edu.cn or jfzhou@tjh.tjmu.edu.cn.

doi: 10.1158/1078-0432.CCR-09-3174

Translational Relevance

Although histone deacetylase inhibitors (HDACi) are emerging as a new class of anticancer agents, one of the most significant concerns is that interactions with a wide array of substrates using these agents might initiate both therapeutic and undesired protective responses. In fact, HDACi usually display relatively low potency when used as a single agent, and hence, are always empirically used in combination with other agents, and accordingly, are not the optimal application of this class of drugs. In this report, we provide the first evidence that an undesired protective signal is initiated by HDACi and highlight a novel molecular mechanism by which HDACi induces the expression of CD146 as a protective response to offset the antitumor efficacy. On the other hand, targeting CD146 could be exploited as a novel strategy to more effectively kill cancer cells. Our current preclinical approach might accelerate the rational design of an optimal HDACi-containing regimen.

partial responses were achieved when sodium phenyl butyrate was used as a single-agent to treat patients with myelodysplasia or acute myeloid leukemia (n = 49; refs. 5, 6). On the other hand, most current clinical trials are combination studies looking at HDACi in combination with other agents (7, 8). Two phase I studies have shown that the combination of vorinostat with conventional chemotherapeutic agents displays synergistic effects in the treatment of advanced solid malignancies (9, 10). Furthermore, synergism has also been observed with various combinations of HDACi and other agents such as all-trans-retinoic acid and proteasome inhibitors (11–14). All of these combination trials seek to increase the antitumor activity of the treatments. Although these combination strategies follow a rational molecular approach in some cases, in most instances, they are relatively empirical. Accordingly, synergism in antitumor efficacy might be accompanied by adverse effects that are rarely or never seen with HDACi alone such as severe myelosuppression (8). Therefore, revealing the molecular mechanisms underlying the low potency of HDACi is pivotal in determining the optimal application of this class of therapeutic agents.

Using cDNA microarray analysis, we now report that the expression of a number of adhesion molecules is significantly induced in HDACi-treated tumor cells both *in vitro* and *in vivo*, of which the induction of CD146 expression was the most significant. CD146 is one of the adhesion molecules belonging to the immunoglobulin superfamily (15). In many types of cancer, including melanoma (16–18), prostate cancer (19–21), and ovarian cancer, elevated expression of CD146 promotes tumor progression and is associated with poor prognosis. Previously, targeting CD146 with antibody against the molecule has been shown to inhibit tumor growth and angiogenesis in several types of cancer. Based on these findings (16, 22, 23), we chose to explore whether the induced expression of CD146 protected tumor cells from HDACi-induced death. We further tested whether the antitumoral activity of HDACi could be significantly enhanced in combination with the targeting of CD146.

Materials and Methods

Cells

Human leukemia (Molt-4), lymphoma (Raji), multiple myeloma (RPMI 8226), and mouse tumor (TC-1) cell lines were cultured in RPMI 1640 supplemented with 10% FCS. Human cervical carcinoma (HeLa), hepatocellular carcinoma (HepG2), ovarian carcinoma (A2780), and human bronchial epithelial BEAS-2B cell lines were cultured in DMEM (Life Technologies) supplemented with 10% FCS. Human breast carcinoma cell line MCF-7 and T47D were cultured in DMEM supplemented with 5% FCS and 10^{-11} mol/L of estradiol during treatment. The breast epithelial cell line MCF-10A was cultured in DMEM/F12 supplemented with 20 ng/mL of epidermal growth factor, 100 ng/mL of cholera toxin, 0.01 mg/mL of insulin, 500 ng/mL of hydrocortisone, and 5% horse serum. All of the cell lines were purchased from American Type Culture Collection.

Reagents and antibodies

HDACi trichostatin A (TSA) and suberoylanilide hydroxamic acid (vorinostat) were purchased from Sigma-Aldrich, Co. The anti-CD146 mouse monoclonal antibody (mAb), AA98, was kindly provided by Dr. Xiyun Yan (Institute of Biophysics, Chinese Academy of Sciences, Beijing, China; ref. 24). FITC anti-CD146 was purchased from eBioscience, Inc. Isotype-matched IgG was purchased from Sigma-Aldrich. Anti-CD31, anti-CD34, anti–E-cadherin, anti–β-catenin, anti-integrin β1, anti–VCAM-1, and anti–β-actin mouse mAbs were purchased from Santa Cruz Biotechnology, Inc. Anti–ICAM-1 mouse mAb was purchased from BD Biosciences. Anti–Ki-67 mouse antibody, clone MIB-1, was purchased from Dako. Anti-acetylated histone H3 or H4 rabbit polyclonal antibodies were purchased from Upstate Biotechnology, Inc. Anti-total Akt, anti-phosphorylated Akt, anti-phosphorylated GSK3β, anti-phosphorylated 4E BP1 rabbit mAb, and anti-phosphorylated S6K1 mouse mAbs were purchased from Cell Signaling Technology, Inc. Triciribine was purchased from Cayman Chemical, Co. Full-length AKT2 cDNA was cloned into pcDNA3.1 plasmid and named as AAkt2 vector, which has been described previously (25).

cDNA microarray analysis

Identification of potential differences in TSA-induced gene expression by Affymetrix GeneChip array analysis: total RNA was extracted from Molt-4 cells cultured in the presence of 0.65 μmol/L of vorinostat for 0, 6, 12, or 24 hours and was subsequently subjected to oligonucleotide microarray analysis. The Affymetrix GeneChip

Human Genome U133 plus 2.0 Array (HG-U133 plus 2.0) was used for the current study (26). This array comprises 1,300,000 unique oligonucleotide probes covering over 47,000 transcripts and variants, which represent approximately 39,000 of the best-characterized human genes. The computer software that accompanied the microarray (Suite 5 analysis software, Affymetrix) was used to process the data from the genechips. We retained only genes with a fold change of at least 2.0 or no more than −2.0 and a *P* value of less than 0.05 (paired *t* test) at 6, 12, and 24 hours after vorinostat treatment. The indicated gene symbols were derived from the NCBI GenBank database.

Quantitative real-time PCR

Quantitative PCR was done in an ABI Prism 7000 using the SYBR Green PCR Master Mix (Sigma) as our previous description (27) with the following set of primers: CD146, 5′-CAG TCC TCA TAC CAG AGC CAA CAG-3′ and 5′-GGA CCA GGA TGC ACA CAA TCA-3′; E-cadherin, 5′-GGA TTG CAA ATT CCT GCC ATT C-3′ and 5′-AAC GTT GTC CCG GGT GTC A-3′; β-catenin, 5′-AAC GTT GTC CCG GGT GTC A-3′ and 5′-GGC AAG ATT TCG AAT CAA TCC AAC-3; integrin β1, 5′-GCC TTA CAT TAG CAC AAC ACC-3′ and 5′-CAT CTC CAG CAA AGT GAA AC-3; ICAM-1, 5′-CCT GAT GGG CAG TCA ACA GCT A-3′ and 5′-ACA GCT GGC TCC CGT TTC A-3′; VCAM-1, 5′-CGT GAT CCT TGG AGC CTC AAA TA-3′ and 5′-GAC GGA GTC ACC AAT CTG AGC A-3′; selectin-E, 5′-CAC TCA AGG GCA GTG GAC ACA-3′ and 5′-CAG CTG GAC CCA TAA CGG AAA C-3′; 18S, 5′-AGT CCC TGC CCT TTG ACA CA-3′ and 5′-GAT CCG AGG GCC TCA CTA AAC-3′. 18s RNA was used as an internal control.

Western blot

Detection of CD146 protein by nonreducing SDS-PAGE was done following the previous description (24). Detection of other proteins by reducing SDS-PAGE was done as described previously (28).

Soft agar colony-forming assay

Cells were treated with mAb AA98 (5 μg/mL for Molt-4, 10 μg/mL for HeLa, HepG2, or MCF-7) + DMSO, vorinostat (0.3 μmol/L for Molt-4, 2.5 μmol/L for HeLa, HepG2, or MCF-7) + isotype-matched mIgG or vorinostat + mAb AA98 for 24 hours. DMSO-treated cells were used as a negative control. A total of 1×10^3 cells were then plated in 60-mm culture plates in medium containing 0.3% agar overlying a 0.5% agar layer. The cells were subsequently incubated for 14 days at 37°C and colonies were stained with 0.5 mL of 0.0005% crystal violet solution for 1 hour and counted using a dissecting microscope (×50 magnifications). The results are expressed as a percentage of colonies in the DMSO-treated group.

Chicken chorioallantoic membrane angiogenesis assay

Fertilized eggs were incubated at 37°C at 65% to 70% humidity. A window of approximately 7 to 10 mm in diameter was cut into the egg shell of 6-day-old embryos, resealed with transparent film, and incubated for a further 2 days. Small filter disks carrying an extremely low dose of 2.5 μg mAb AA98, 2.64 pg vorinostat + isotype-matched mIgG, or vorinostat + mAb AA98 were separately applied to the chorioallantoic membrane (CAM) of individual embryos. DMSO was used as a negative control. Ten eggs were used in each group. After 72 hours of incubation, neovascularization in chicken CAMs was observed and images were acquired with a digital photomicroscope (Olympus). The number of small branching capillaries was counted within a defined area of 72 mm^2 surrounding the implanted disc. In each group, 10 embryos were used and the data represent the mean ± SD.

Animal experiments

Female athymic BALB/c nude mice were obtained from the Animal Center of the Chinese Academy of Medical Science (Beijing, China). The 6-week-old mice used were maintained in a laminar-flow cabinet under specific pathogen–free conditions. In tumor xenograft models, 1×10^7 HeLa or HepG2 cells were injected s.c. into the back of mice. Once tumors had grown to 5 to 6 mm, the mice were grouped ($n = 10$) and administered i.p. with 8 mg/kg of mAb AA98 or 20 mg/kg of vorinostat + isotype-matched mIgG or vorinostat + mAb AA98 twice a week until the mice were sacrificed (tumor volume >1,000 mm^3 or 42 d after treatment). PBS served as a control. Tumor size was measured twice a week and tumor volume was determined according to the equation: tumor size = $\text{width}^2 \times \text{length} \times (\pi/6)$.

In the second portion of the animal studies, an experimental model of transplantable B-lymphoma in TA2 mice was established. TA2 mice were obtained from the Animal Experimental Center of the Tianjin Cancer Institute (Tianjin, China). The model was derived from spontaneous lymphoma in a TA2 mouse and remained stable past 43 generations by successful transplantations in TA2 mice over 4 years. The model grows rapidly and eventually develops invasive metastases in all mice. Transplantable B-lymphoma tissues were cut into small 1 mm^3 pieces and lymphoma cells were dissociated by digestion with collagenase type I. Female 4-week-old TA2 mice were inoculated with 5×10^5 lymphoma cells into the inguinal groove muscle. Following inoculation, mice were then grouped ($n = 8$) and administered intratumorally with 5 mg/kg of mAb AA98 or i.p. with 15 mg/kg of vorinostat + isotype-matched mIgG, or vorinostat + mAb AA98 twice a week. PBS served as a control. The onset of the primary tumor was defined as a tumor diameter of more than 0.2 cm^3 and the dissemination of lymphoma was defined as a remote lymph node diameter over 0.2 cm^3. The growth and dissemination of lymphoma was monitored weekly until the mice were sacrificed (30 d after inoculation).

In the final portion of the animal studies, a mouse corneal tumor model was established. C57Bl/6 mice were obtained from the Animal Center of the Chinese Academy of Medical Science. First, 5×10^6 TC-1 cells were injected s.c. in the flanks of C57Bl/6 mice and the tumors

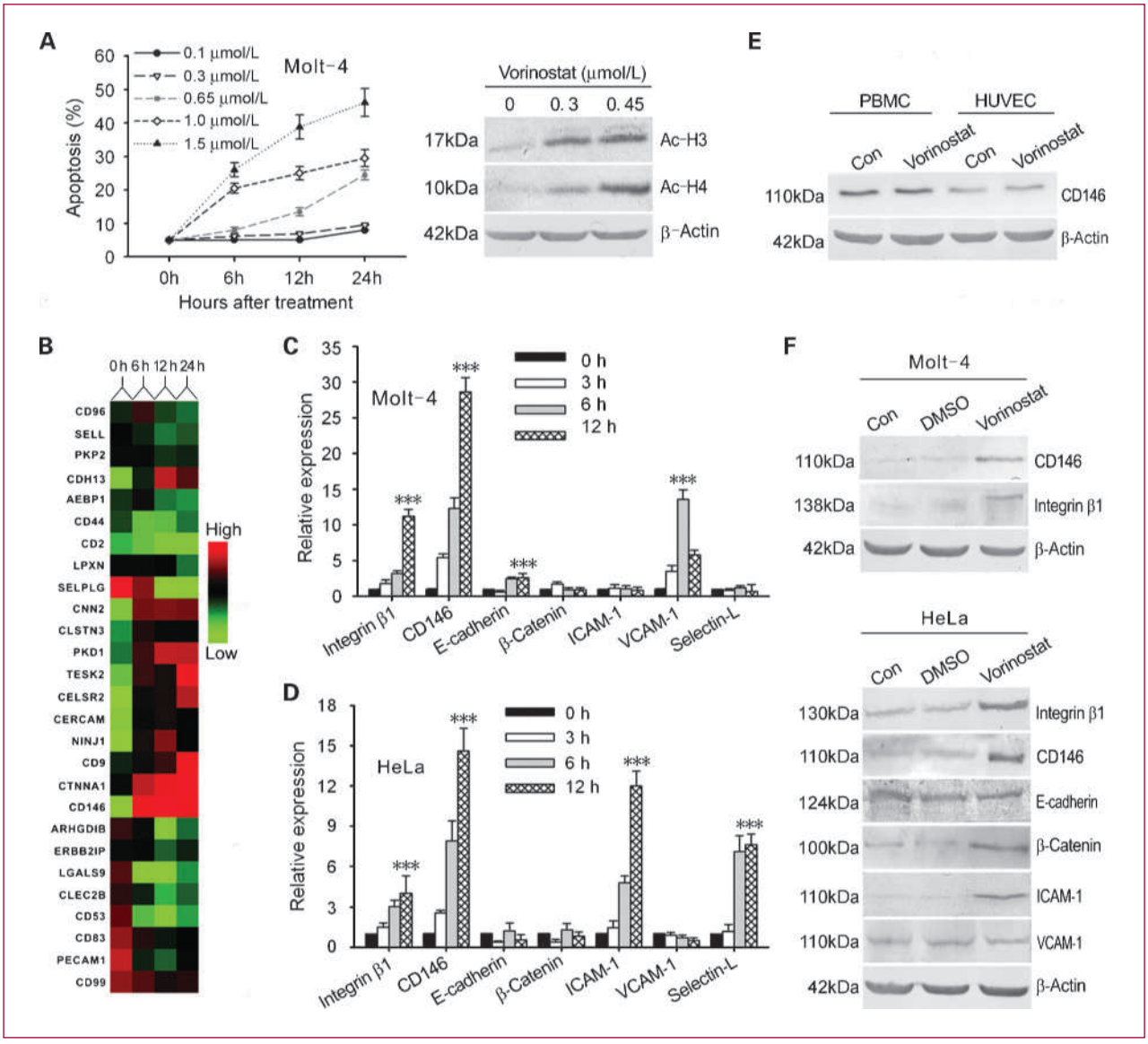

Fig. 1. Vorinostat induces the expression of adhesion molecules in Molt-4 and HeLa cells. A, Molt-4 cells were suspended in the presence of vorinostat at the indicated concentrations and assayed at 0, 6, 12, and 24 h for apoptosis and levels of acetylation of histones H3 and H4. The percentage of apoptotic cells was monitored by Annexin V/PI staining (left). After a 24-h exposure to the designated concentration of vorinostat, the cells were analyzed by Western blot for the levels of acetylation of histones H3 and H4 (right). B, expression profiling data were presented as a heatmap using CLUSTER and TREEVIEW software. Significant changes of adhesion molecule expression were detected after the addition of vorinostat at the indicated hours. In Molt-4 cells (C) and HeLa cells (D), the expression of seven representative adhesion molecules was determined by quantitative real-time PCR before and after treatment of vorinostat. Each data point represents the mean ± SD of three replicates. Results are normalized to those of 18s RNA and are expressed as the fold induction compared with the 0 h group. The transcriptional level for the 0 h group is set as 1 (***, $P < 0.001$). E, peripheral blood mononuclear cells and human umbilical vein endothelial cells were treated with PBS or 2.5 μmol/L of vorinostat for 24 h before examination of CD146 protein. F, after treatment with vorinostat for 24 h, the protein levels of representative adhesion molecules were determined.

were allowed to grow to 7 to 8 mm. The mice were then sacrificed and the tumors were collected and cut into several small pieces. Next, implantation of one piece of TC-1 tumor tissue in the mouse cornea was carried out according to previously described procedures (29). After implantation, the mice were grouped ($n = 6$) and 8 mg/kg of mAb AA98, 20 mg/kg vorinostat + isotype-matched mIgG, or vorinostat + mAb AA98 was applied to the eye twice daily for 2 weeks. PBS served as a control. The corneas were then collected for immunofluorescence evaluation.

Laser scanning cytometry

Laser scanning cytometry (LSC) slides were scanned using an LSC instrument equipped with an argon (Ar; 488 nm) and helium-neon (HeNe; 633 nm) laser and iCys3.3.4 software (CompuCyte). DNA staining based

on hematoxylin served as the trigger/contouring parameter. The following channels and settings were used for data collection: argon green (PMT, 15-25%; offset, 0.2; gain, 13%), HeNe LongRed (LR; PMT, 14-22%; offset, 0-0.3; gain, 13%). We analyzed the immunohistochemical tissue samples in phantom mode. Argon green and HeNe LongRed parameters were collected with compensation. Statistical analysis was done on the results of three independent experiments using the paired Student's *t* test.

Statistical analysis

The statistical significance of differences between experimental and control groups was determined by one-way ANOVA followed by the Student-Newman-Keuls test using SPSS software version 13.0 (SPSS, Inc.). Kaplan-Meier analyses were done for the survival studies and statistical significance was measured by using the log rank test. All statistical tests were two sided, and $P < 0.05$ was considered statistically significant.

Results

Vorinostat induces the expression of adhesion molecules in Molt-4 and HeLa cells

We determined the kinetics and dosage range of vorinostat-induced apoptosis in Molt-4 cells. Molt-4 cells were incubated for different time with vorinostat at various doses before apoptosis was determined. The dose range of vorinostat was between 0.1 and 1.5 μmol/L based on earlier pharmacokinetics studies and the fact that

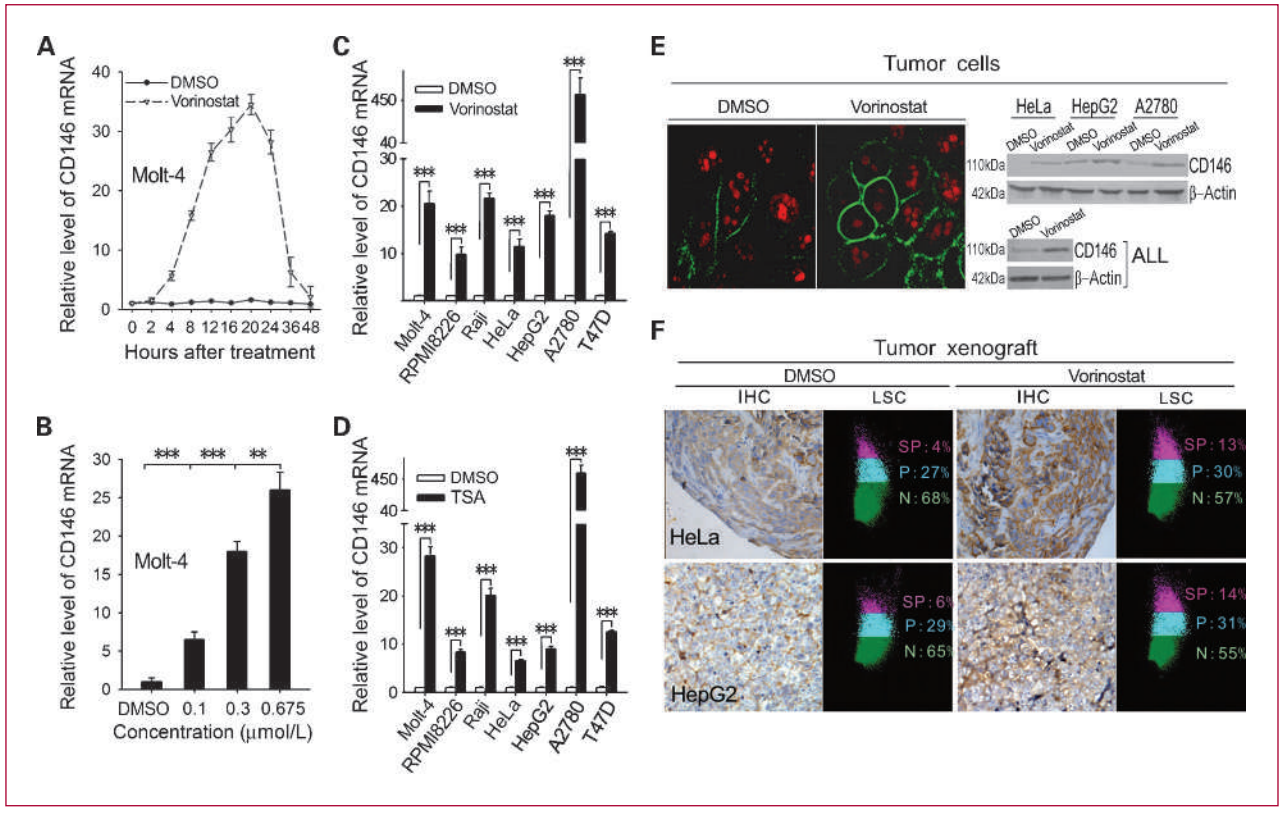

Fig. 2. Induction of CD146 is a common phenomenon in vorinostat-treated cancer cells both *in vitro* and *in vivo*. A, Molt-4 cells were treated with 0.45 μmol/L of vorinostat or DMSO for the indicated times. After treatment, the mRNA level of CD146 was analyzed by quantitative real-time PCR. Each data point represents the mean ± SD of three replicates. Results are normalized to those of 18s RNA and are expressed as the fold induction compared with the 0 h group. The transcriptional level for the 0 h group is set as 1. B, Molt-4 cells were treated with vorinostat at the indicated concentrations for 12 h and the mRNA level of CD146 was analyzed by quantitative real-time PCR as above (**, $P < 0.01$; ***, $P < 0.001$, as compared with the DMSO-treated group). C, seven tumor cell lines representative of different tissue origins were treated with vorinostat or DMSO (0.5 μmol/L for Molt-4; 5 μmol/L for all the other six cell lines for 24 h). The mRNA level of CD146 was analyzed by quantitative real-time PCR (***, $P < 0.001$). D, seven tumor cell lines representative of different tissue origins were treated with TSA (0.1 μmol/L for Molt-4; 0.5 μmol/L for all the other six cell lines for 24 h). The mRNA level of CD146 was analyzed by quantitative real-time PCR (***, $P < 0.001$). E, HeLa cells were treated with 2.5 μmol/L of vorinostat or DMSO for 12 h and were then analyzed by immunofluorescent analysis for staining of CD146, representative images under a confocal microscope (magnification, ×600). Top, tumor cell lines (HeLa, HepG2, A2780) were treated with 2.5 μmol/L of vorinostat or DMSO for 24 h and analyzed for protein levels of CD146. Bottom, freshly isolated acute lymphoblastic leukemia cells were treated with 0.45 μmol/L of vorinostat or DMSO for 24 h and analyzed for protein levels of CD146 (ALL, acute lymphoblastic leukemia). F, HeLa and HepG2 tumor-bearing mice were treated with 25 mg/kg of vorinostat or DMSO for 24 h and CD146 expression was determined by immunohistochemistry and quantified by LSC. Images represent typical data (SP, strong positive; P, positive; N, negative). Total positive rate for CD146 (SP plus P) is the mean ± SD ($n = 10$).

Table 1. Effect of vorinostat on the expression of CD146 in clinical tumor samples

Patients	Clinical diagnosis	Classification	Time course (h)			
			0	3	6	12
Patient 1	Leukemia	ALL	1	6.63 ± 0.28	5.78 ± 0.15	1.33 ± 0.02
Patient 2	Leukemia	ALL	1	8.76 ± 1.33	15.14 ± 3.25	13.42 ± 2.16
Patient 3	Leukemia	AML	1	12.15 ± 3.05	18.46 ± 4.23	10.18 ± 2.55
Patient 4	Leukemia	CML	1	27.28 ± 2.26	26.53 ± 2.14	27.28 ± 3.54
Patient 5	Leukemia	CLL	1	25.98 ± 4.65	28.48 ± 3.92	28.13 ± 3.15
Patient 6	Lymphoma	HD	1	8.24 ± 1.36	16.93 ± 2.57	12.66 ± 2.25
Patient 7	Lymphoma	NHL	1	7.52 ± 0.84	20.11 ± 3.11	11.55 ± 2.03
Patient 8	Lymphoma	NHL	1	9.22 ± 1.78	21.56 ± 3.35	18.65 ± 2.61
Patient 9	Myeloma	Multiple	1	8.35 ± 0.93	15.70 ± 2.64	13.22 ± 2.13
Patient 10	Ovarian cancer	Serous	1	77.2 ± 9.36	16.19 ± 1.56	16.83 ± 2.87

NOTE: Data are expressed as fold increase (mean ± SE) of CD146 mRNA from vorinostat-treated cells relative to that from medium-treated cells. Each data was analyzed at least in three independent experiments.
Abbreviations: ALL, acute lymphoblastic leukemia; AML, acute myelocytic leukemia; CML, chronic myelocytic leukemia; CLL, chronic lymphocytic leukemia; HD, Hodgkin disease; NHL, non-Hodgkin lymphoma.

vorinostat at these doses is physiologically tolerable (30). Vorinostat at concentrations of 0.3 μmol/L or above displayed obvious HDACi activity as defined by significant acetylation of histones H3 and H4 (Fig. 1A). Vorinostat-induced apoptosis was detectable at 6 hours and reached a maximum at 24 hours in a dose-dependent fashion (Fig. 1A). To identify the potential genes critical for protecting cells from vorinostat-induced apoptosis, Molt-4 cells were treated with 0.65 μmol/L of vorinostat for 0, 6, 12, or 24 hours prior to cDNA microarray analysis. The expression of about 130 genes was found to be at least 2-fold increased or decreased at 6, 12, and 24 hours after vorinostat treatment. These genes cover a wide range of cellular functions. Interestingly, among these genes, a total of 27 genes (20.8%) belong to the adhesion molecule gene superfamily (Fig. 1B; Supplementary Table S1). To validate the microarray data, the expression of seven well-known adhesion molecules that belong to four major classes of adhesion molecules was examined in vorinostat-treated Molt-4 and HeLa cells. Although the expression of some adhesion molecules such as ICAM-1, VCAM-1, and Selectin-L was induced by vorinostat in a cell-specific manner, upregulated expression of integrin β1 or CD146 was consistently detected in both vorinostat-treated Molt-4 (Fig. 1C) and HeLa (Fig. 1D) cells. To observe the effect of vorinostat on normal cells, peripheral blood mononuclear cells and human umbilical vein endothelial cells were treated with PBS or vorinostat (2.5 μmol/L) for 24 hours, the protein expression of CD146 was not induced by vorinostat in either peripheral blood mononuclear cells or human umbilical vein endothelial cells (Fig. 1E). To test whether vorinostat-induced transcription gave rise to the elevated protein levels, protein abundance was determined 24 hours after vorinostat treatment. Again, 0.65 μmol/L vorinostat significantly elevated protein levels of integrin β1 and CD146 in both Molt-4 and HeLa cells (Fig. 1F).

Induction of CD146 is a common phenomenon in vorinostat-treated cancer cells both *in vitro* and *in vivo*

We selected CD146 for further study because it is the most significantly upregulated adhesion molecule following vorinostat treatment. In addition, previous publications have linked CD146 with apoptosis resistance in cancer cells (31–33). We initially examined the time pattern of vorinostat-induced CD146 mRNA expression in Molt-4 cells. The induction was detectable in as early as 4 hours and reached a maximum at 20 hours after vorinostat treatment. Vorinostat-induced expression of CD146 lasted up to 48 hours before decreasing to baseline levels (Fig. 2A). Obviously, the expression of CD146 was induced in a vorinostat dose-dependent manner (Fig. 2B). Next, we examined whether vorinostat consistently induced the expression of CD146 in cancers of different tissue origins. In all six tumor cell lines, including RPMI 8226, Raji, HeLa, HepG2, A2780, or T47D, vorinostat consistently induced the transcription of CD146 (Fig. 2C). Furthermore, another HDACi, TSA, significantly induced the expression of CD146, indicating that the induction of CD146 expression might be a common action shared by HDACi (Fig. 2D). To determine whether the vorinostat-induced expression of CD146 occurs in primary tumor cells, 10 primary tumor samples from patients with leukemia, lymphoma, multiple myeloma or ovarian cancer were treated with vorinostat. Again, vorinostat significantly induced the expression of CD146 as early as 3 hours after treatment and the increase lasted up to 12 hours in all of the samples examined (Table 1). To address whether the induction of CD146 transcription gave rise to the upregulated level of CD146 protein, cultured HeLa cells were

treated with vorinostat or DMSO and examined for the CD146 protein using immunofluorescence. As expected, treatment of vorinostat significantly enhanced the positive immunoreactivity of CD146 in HeLa cells (Fig. 2E, left). The increased expression of CD146 protein was also confirmed by Western blotting in three cell lines (Fig. 2E, top right). Furthermore, the induction of CD146 gave rise to elevated expression levels of CD146 protein in a primary acute lymphoblastic leukemia sample (Fig. 2E, bottom right). The vorinostat-induced expression of CD146 protein was further confirmed by flow cytometry analysis in other primary samples from patients with acute lymphoblastic leukemia, acute myeloid leukemia, or chronic myelogenous leukemia (Supplementary Fig. S1).

To address whether the induction of CD146 occurs *in vivo*, HeLa and HepG2 tumor-bearing mice ($n = 10$) were treated with vorinostat at 25 mg/kg based on earlier studies (34, 35). Similarly, CD146 expression was remarkably elevated in the tumor cell membrane 24 hours after treatment with vorinostat, as determined by immunohistochemistry and quantified by LSC (Fig. 2F); total positive rate for CD146 of HeLa tumor treated with vorinostat versus treated with DMSO: 41 ± 2% versus 32 ± 1%, $P < 0.05$; total positive rate for CD146 of HepG2 tumor treated with vorinostat versus treated with DMSO: 44 ± 2% versus 36 ± 1%, $P < 0.05$.

Targeting CD146 substantially enhanced vorinostat-induced killing via suppression of the Akt pathway in cancer cells

To understand the significance of vorinostat-induced CD146 expression in cancer cells, we chose AA98, an anti-CD146 mAb, to selectively target CD146 (24). Whereas AA98 alone did not induce significant apoptosis with

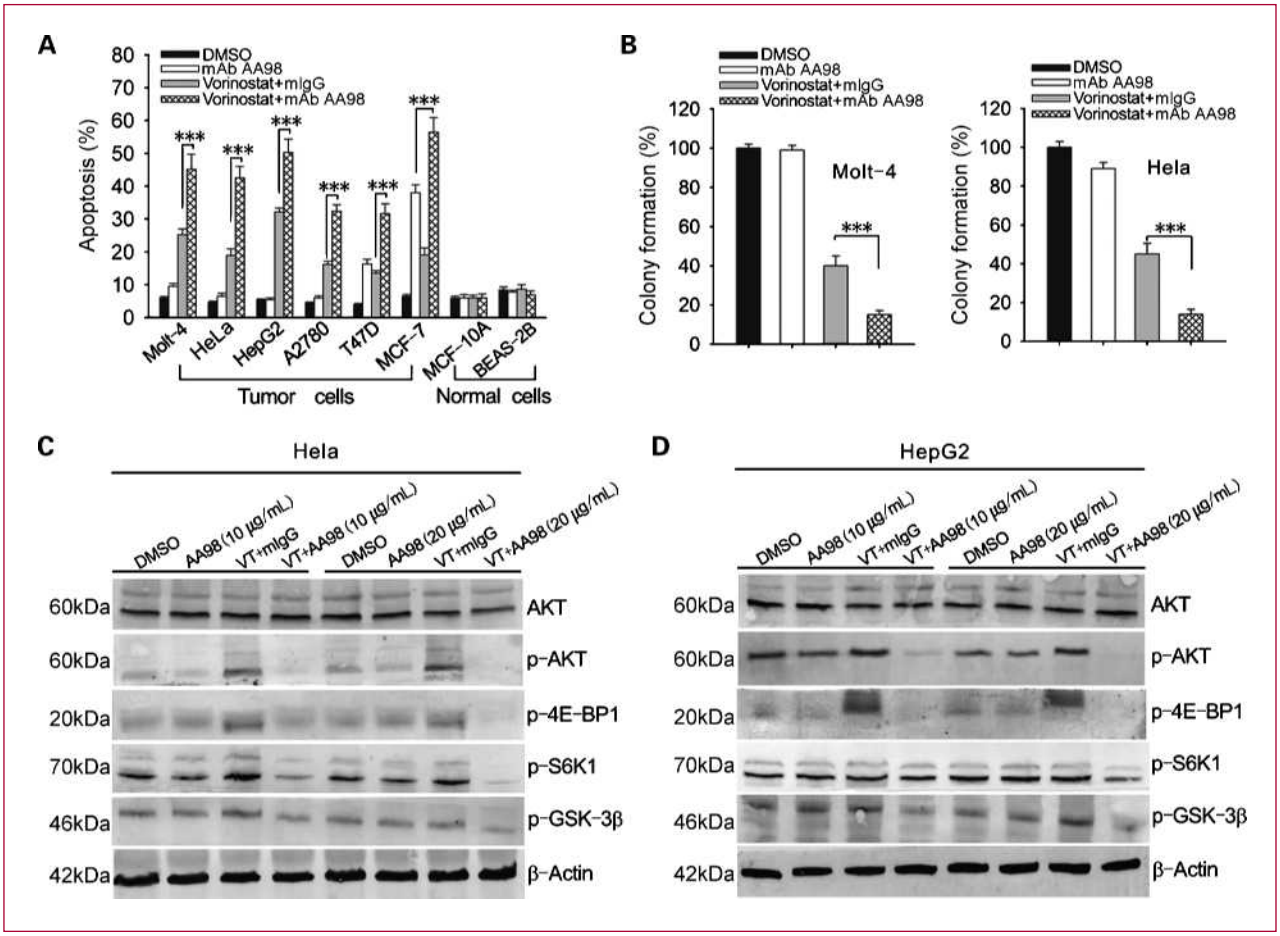

Fig. 3. Targeting CD146 substantially enhanced vorinostat-induced death via suppression of the Akt pathway in cancer cells. A, tumor and nonmalignant cells were exposed to mAb AA98 (10 μg/mL for Molt-4; 20 μg/mL for all the other seven cell lines), vorinostat (0.5 μmol/L for Molt-4; 5 μmol/L for all the other seven cell lines), or both agents for 48 h and subjected to apoptosis analysis using flow cytometry. Each data point represents the mean apoptosis ± SD of three replicates (***, $P < 0.001$). B, cells were treated with mAb AA98 (5 μg/mL for Molt-4, 10 μg/mL for HeLa) or vorinostat (0.3 μmol/L for Molt-4, 2.5 μmol/L for HeLa) + isotype-matched mIgG, or vorinostat + mAb AA98 for 24 h and then subjected to the soft agar colony-forming assay (***, $P < 0.001$). Results are expressed as a percentage of colonies in the DMSO-treated group. Each data point represents the mean ± SD of three replicates. HeLa (C) and HepG2 (D) cells were treated as depicted for 24 h and examined for protein levels of total Akt, p-Akt, p-4E-BP1, p-S6K1, p-GSK-3β, and β-actin. VT, vorinostat treatment (5 μmol/L for all the cell lines).

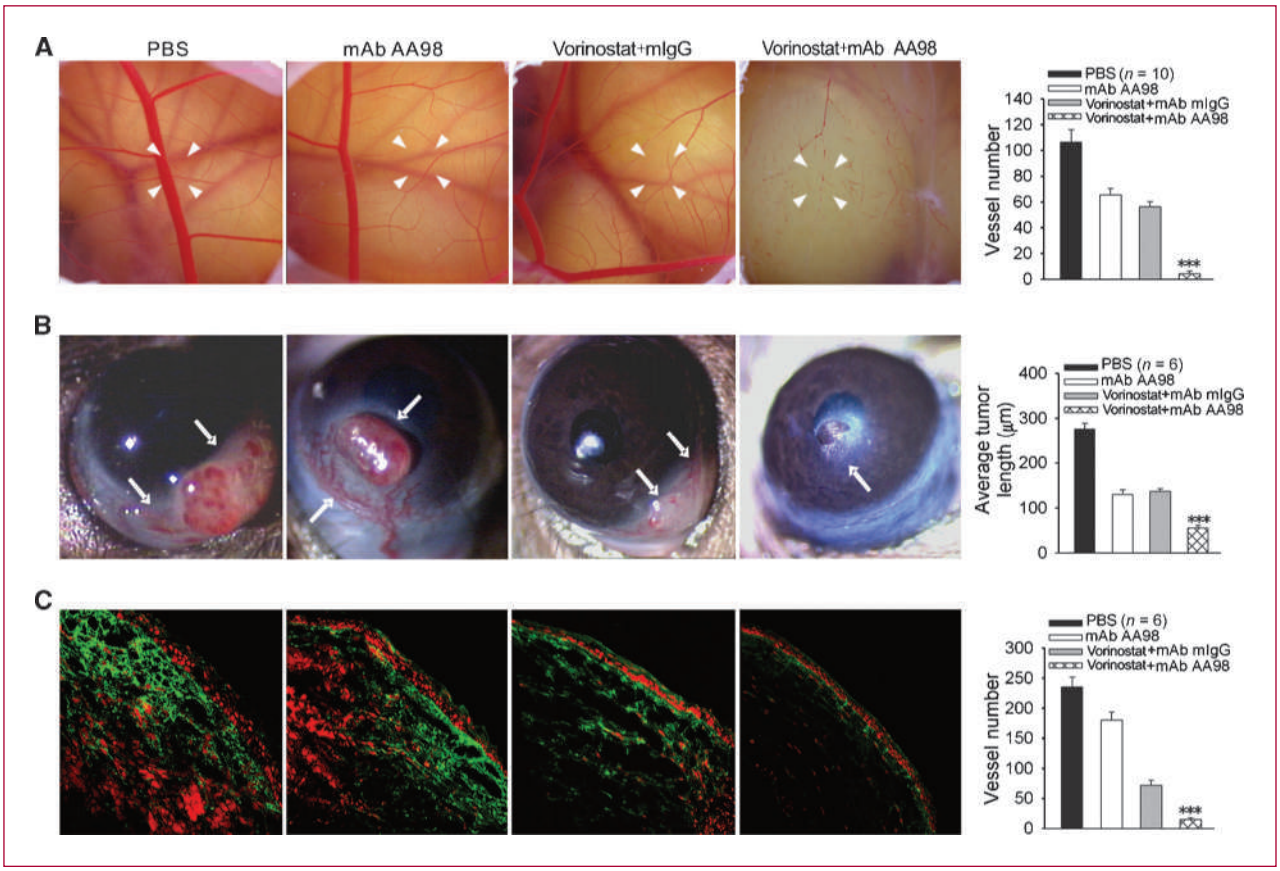

Fig. 4. Combination of HDACi with CD146 mAb has synergistic antiangiogenic effects. A, the CAM of individual embryos was treated with small filter disks carrying PBS, 2.5 μg mAb AA98, 2.64 pg vorinostat + isotype-matched mIgG, or vorinostat + mAb AA98. After 72 h of incubation, neovascularization in chicken CAM was determined. Left, representative images of neovascularization in chicken CAM. Right, quantitative data of neovascularization in chicken CAM. The data represent the mean ± SD of 10 embryos. B, for mouse corneal tumor model, one piece of TC-1 tumor tissue was implanted into the mouse cornea. Mice were grouped (n = 6) and treated with 8 mg/kg of mAb AA98, 20 mg/kg of vorinostat + isotype-matched mIgG, or vorinostat + mAb AA98 to the eye twice daily for 2 wk. Corneas were collected for determination of average corneal tumor length and angiogenesis. Left, typical results of mouse corneal tumor after treatment. Newly formed vessels were indicated by white arrows. Right, quantitative data of average corneal tumor length. Each data represents the mean ± SD of six samples (***, $P < 0.001$). C, cornea tumor sections were stained with CD34 (red) and analyzed for the average blood vessels under a confocal microscope, only the vessels with intact cross-sectional view were calculated. Left, typical results of angiogenesis in corneal tumors after treatment. Right, each data point represents the mean ± SD (n = 6; ***, $P < 0.001$).

the exception of T47D and MCF-7 cells, it substantially sensitized cancer cells to vorinostat-induced apoptosis in all the cell lines examined (Fig. 3A). On the other hand, AA98 did not significantly sensitize nontransformed cells (MCF-10A, BEAS-2B) to vorinostat-induced cell death (Fig. 3A). These results were further supported by a quantitative colony-forming assay. AA98 synergized with vorinostat to significantly reduce tumor colonies in Molt-4 and HeLa cells (Fig. 3B). Moreover, AA98 alone or in combination with vorinostat significantly inhibited tumor colonies in tumor cell lines (HepG2, T47D, and MCF-7) in which AA98 showed significant killing activity (Supplementary Fig. S2). To further confirm that targeting of CD146 sensitizes tumor cells to HDACi treatment, CD146 expression was knocked down in HeLa or HepG2 cells prior to vorinostat treatment (Supplementary Fig. S3A). Although CD146 RNAi alone did not significantly induce apoptosis, it substantially sensitized tumor cells to vorinostat-induced apoptosis (Supplementary Fig. S3B and C). Because data previously showed a link between CD146 expression and Akt activation (33, 36), we sought to determine the effects of vorinostat/AA98 on the Akt pathway in HeLa and HepG2 cells. Vorinostat induced the phosphorylation of AKT and downstream targets, and AA98 coadministration reverses the activation of AKT pathway induced by vorinostat in a dose-dependent manner (Fig. 3C-D). To further confirm whether Akt really had a protective effect on vorinostat/AA98 induced apoptosis, overexpression/inhibition experiments had been done by using AAkt2 plasmid transfection or triciribine treatment. Although transfection of AAkt2 inhibited vorinostat/AA98-induced apoptosis, the inhibition of Akt phosphorylation by triciribine substantially sensitized HeLa cells to vorinostat/AA98-induced killing (Supplementary Fig. S4). To answer whether the synergy of anti-CD146 was limited to HDACi or more generally to other

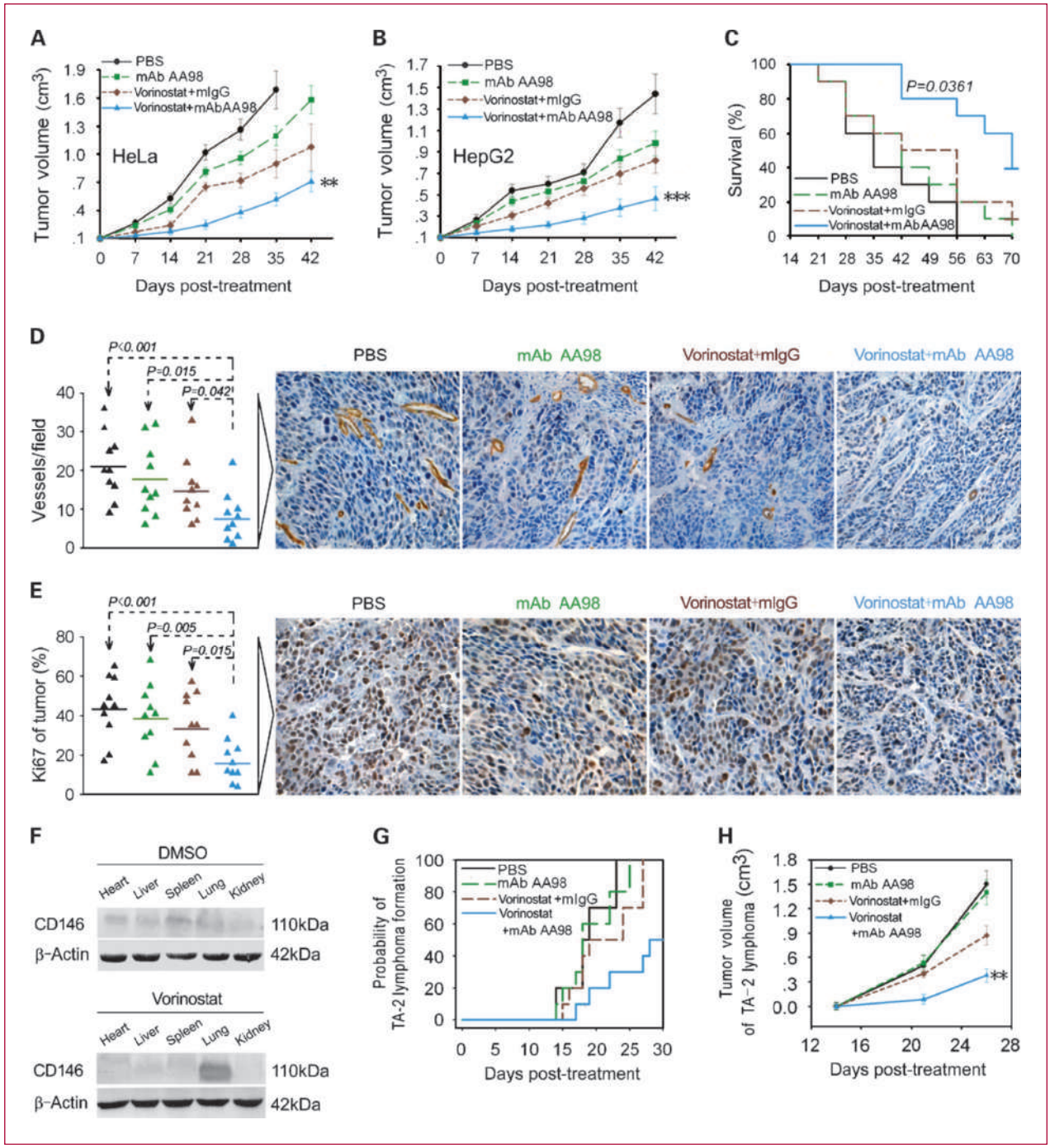

Fig. 5. Combination of HDACi with CD146 mAb has synergistic antitumor effects on tumor growth and metastasis *in vivo*. A, when the tumor reached a diameter of 5 to 6 mm, HeLa (A) or HepG2 (B) tumor-bearing mice were grouped (n = 10) and administered i.p. with PBS (black), mAb AA98 (green), vorinostat plus mIgG (brown), or vorinostat plus mAb AA98 (blue). Mean tumor volumes were monitored at specific time points after treatment. Each data point represents mean ± SD (**, $P < 0.01$; ***, $P < 0.001$; n = 10). C, Kaplan-Meier survival curves of HeLa tumor-bearing mice following various treatments as indicated. Each group included 10 animals. D, HeLa tumor-bearing mice were treated with PBS (black), mAb AA98 (green), vorinostat plus mIgG (brown) or vorinostat plus mAb AA98 (blue). Sections of tumors were stained with CD31 (D) or Ki67 (E). Left, quantitative data of novel vessels (D) or Ki67-positive areas (E) per microscope field. Each data point represents the mean of the triplicate microscope field obtained from each tissue sample. Right, representative 200× images. Different treatments were labeled with various colors. PBS. F, expression of CD146 in important organs of C57BL/6 was examined 24 h after treatment with vorinostat or DMSO. G, when TA2 lymphoma reached a diameter of 5 to 6 mm, the TA2 mice were grouped (n = 8) and administered i.p. with PBS (black), mAb AA98 (green), vorinostat plus mIgG (brown) or vorinostat plus mAb AA98 (blue) twice a week for 26 d. The cumulative probability of tumor formation was determined by the appearance of neoplasms in the inguinal groove muscle and (H) tumor volume was monitored. Each data point represents mean ± SD (**, $P < 0.01$).

chemotherapeutic agents, HeLa cells were treated by AA98 in combination with cisplatin and subjected to apoptosis analysis. In contrast to AA98 plus vorinostat, AA98 did not significantly sensitize HeLa to cisplatin-induced cell death, and failed to suppress AKT phosphorylation (Supplementary Fig. S5).

Targeting CD146 synergized with vorinostat to inhibit angiogenesis

Because both vorinostat and anti-CD146 mAb have been previously reported to inhibit angiogenesis (15, 37, 38), we next examined whether targeting CD146 would synergize with vorinostat to inhibit angiogenesis. Although an extremely low dose of 2.5 μg of AA98 or 2.64 pg of vorinostat failed to inhibit angiogenesis in the CAM assay, a combination of the two agents completely abolished angiogenesis (Fig. 4A). In four independent experiments, the combination of AA98 with vorinostat consistently showed over 10-fold more potent inhibition of angiogenesis than either AA98 or vorinostat alone (Fig. 4A; Supplementary Table S2). Next, a tumor-associated angiogenesis model was used to test whether the combination would inhibit tumor-induced angiogenesis. The corneal tumor angiogenesis model is considered one of the best *in vivo* models. The cornea itself is avascular. Thus, any vessels seen in the cornea after tumor implantation are new vessels. The progress of angiogenesis and vascular response can be monitored by direct observation (39, 40). As shown in Fig. 4B, implantation of tumor tissues into the corneal micropockets resulted in the growth of tumors expanding from the micropockets to the limbus. Corneal tumor neovascularization became directly visible by gross examination 2 weeks after implantation. These newly formed tumor vessels, sprouting from the limbal vessels, infiltrated the entire area of the tumor tissue. Treatment with mAb AA98 slowed down tumor growth, but had no obvious effect on angiogenesis, whereas vorinostat + mIgG seemed to be a potent inhibitor of angiogenesis in the corneal tumor. It is of note that the combined treatment with vorinostat and mAb AA98 resulted in an almost complete loss of tumor blood vessels and retardation of tumor growth. Immunofluorescence analyses of corneal tissues using an anti-CD34 antibody confirmed the differences in vascular density caused by the different treatments (Fig. 4C; ***, $P < 0.001$). Collectively, these data showed the targeting of CD146 through synergism with vorinostat to substantially inhibit angiogenesis.

Targeting CD146 synergized with vorinostat to substantially inhibit tumor growth and metastasis *in vivo*

To determine the *in vivo* antitumor efficacy of combined vorinostat and AA98, we chose lower doses of the two agents than those previously reported (24, 34). In the first portion of the animal study, when the tumor reached a diameter of 5 to 6 mm, HeLa or HepG2 tumor bearing mice were grouped ($n = 10$) and administered i.p. with AA98 or vorinostat. Although no tumor complete regression was observed in any groups with different treatments, tumor growth was significantly retarded in the group with combined vorinostat and AA98 (Fig. 5A and B). Furthermore, combined vorinostat and AA98 significantly improved the survival in HeLa tumor-bearing mice (Fig. 5C; $P = 0.0361$). To further examine the correlation between vascularity and tumor growth, we counted CD31-positive blood vessels in the tumor sections of mice treated for 21 days (Fig. 5D). We observed a more significant reduction of microvessel density in tumors treated with vorinostat + mAb AA98 compared with tumors treated with either drug alone ($P = 0.042$, vorinostat + mAb AA98 versus vorinostat + mIgG; $P = 0.015$, vorinostat + mAb AA98 versus mAb AA98). Furthermore, the proliferation of the tumor as defined by positive staining of the Ki-67 antigen was substantially inhibited by combined vorinostat and AA98 treatment (Fig. 5E). We also tested the effect of vorinostat on major organs of C57BL/6, such as heart, liver, spleen, lung, and kidney. It was showed that the expression of CD146 was only upregulated in the lung after treatment of vorinostat for 24 hours (Fig. 5F).

To determine the effect of combined vorinostat and AA98 on tumor onset and metastasis, a TA2 mouse lymphoma model was used. The model was derived from spontaneous lymphoma in a TA2 mouse and remained stable past 43 generations by successful transplantations in TA2 mice over 4 years. The lymphoma grows rapidly and eventually develops invasive metastases in all mice. Importantly, the combination of vorinostat with mAb AA98 significantly decelerated the formation of lymphoma as compared with vorinostat or mAb AA98 alone (rate of formation of lymphoma in TA2 mice 26 d after vorinostat + mIgG treatment versus vorinostat + mAb AA98 treatment: 70% versus 30%, $P < 0.05$; Fig. 5G). More significantly, we observed the dissemination of lymphoma as defined by the appearance of remote lymph nodes in all PBS-, mAb AA98-, and vorinostat + mIgG–treated mice within 26 days of inoculation. Furthermore, the combination of vorinostat with mAb AA98 significantly inhibited the growth of lymphoma (Fig. 5H), and only four out of eight mice were found to have developed tumors 30 days after inoculation.

Discussion

The targets of HDACi are so extensive that it is not surprising that HDACi would initiate both antiapoptotic and proapoptotic therapeutic responses. In fact, HDACi usually display relatively low potency when used as a single agent. Unfortunately, most of the current HDACi combination strategies are more empirical than mechanism-based applications, and accordingly, are not optimal for this class of drugs (18). The present findings provide the first evidence that an undesired protective signal is initiated by HDACi and highlight a novel molecular mechanism by which HDACi induces the expression of CD146 as a protective response to offset the

antitumor efficacy. On the other hand, the induction of CD146 could be exploited as a novel strategy for the enhanced killing of cancer cells, but not nontransformed cells. Considering that HDACi could modulate the expression of a large amount of genes, the induction of molecules other than CD146 might serve as a generally applicable strategy for the optimal design of HDACi-containing regimens. The findings presented here argue that dissecting the HDACi-induced programs is fundamentally important for a mechanism-based combined application of HDACi with other agents.

In the present study, the expression of a large number of adhesive molecules was induced by treatment with HDACi in a cell type–specific pattern. Previously, other investigators had shown HDACi-induced expression of adhesion molecules on acute myeloid leukemia cells including CD86 as well as ICAM-1 (41). Interestingly, the induction of CD146 or integrin β1 is a common phenomenon in vorinostat-treated cancer cells. On the other hand, targeting CD146 with antibody had been shown to inhibit tumor growth and angiogenesis (24). In our hands, AA98 alone also showed killing activity in T47D and MCF-7. Although the mechanism underlying the antitumoral activity of AA98 as a single agent is currently unknown, some investigators proposed that the engagement of AA98 with CD146 inhibited tumor metastasis by suppression of p38 mitogen-activated protein kinase phosphorylation and NF-κB activation (15). Nevertheless, the HDACi-induced expression of CD146 as a protective program is a novel finding. Interestingly, targeting CD146 substantially sensitized tumor cells to vorinostat-induced killing. Treatment of vorinostat plus CD146 mAb also preferentially ablates cancer colony formation, whereas nontransformed cells seem largely unaffected. Significantly, the combined regimen of HDACi and CD146 mAb significantly inhibits the activity of the Akt pathway. Recent clinical evaluation of pharmaceutical-grade antibodies and synthetic cyclic RGD peptides against adhesion molecules may soon provide opportunities to test the therapeutic potential of HDACi in combination with such agents. Notably, our present data indicate that the profound inhibitory effect on angiogenesis is likely to be another aspect responsible for the enhanced antitumor efficacy. Given that angiogenesis plays a critical role in the progression of tumors, the potential therapeutic implications of the combination are substantial and attractive in a clinical setting. Currently available antiangiogenic agents have been developed based on the understanding of general rather than tumor-associated angiogenesis. Novel antiangiogenic agents targeting tumor-derived endothelial cells rather than genetically normal endothelial cells are urgently needed. Future studies may further clarify the efficacy of combined HDACi with the targeting of CD146 against tumor-associated angiogenesis as compared with currently available antiangiogenic agents.

Finally, HDACi usually exhibits limited efficacy when used as a single agent. The limitation has spurred the development of a combination of HDACi with other agents for most types of cancers. However, the identification of an optimal HDACi-based regimen requires long-term and painstaking clinical trials and suboptimal application. Our current preclinical approach might accelerate the rational design of an optimal HDACi-containing regimen.

Disclosure of Potential Conflicts of Interest

No potential conflicts of interest were disclosed.

Grant Support

National Science Foundation of China (nos. 30700895, 30770913, 30770914, 30801224, and 30528012), NCET-04-0719, and "973" Program (2009CB521800).

The costs of publication of this article were defrayed in part by the payment of page charges. This article must therefore be hereby marked *advertisement* in accordance with 18 U.S.C. Section 1734 solely to indicate this fact.

Received 12/09/2009; revised 07/19/2010; accepted 08/15/2010; published OnlineFirst 09/30/2010.

References

1. Bolden JE, Peart MJ, Johnstone RW. Anticancer activities of histone deacetylase inhibitors. Nat Rev Drug Discov 2006;5:769–84.
2. Marchion D, Munster P. Development of histone deacetylase inhibitors for cancer treatment. Expert Rev Anticancer Ther 2007;7:583–98.
3. Marks PA, Breslow R. Dimethyl sulfoxide to vorinostat: development of this histone deacetylase inhibitor as an anticancer drug. Nat Biotechnol 2007;25:84–90.
4. Lindemann RK, Gabrielli B, Johnstone RW. Histone-deacetylase inhibitors for the treatment of cancer. Cell Cycle 2003;3:779–88.
5. Gore SD, Weng LJ, Figg WD, et al. Impact of prolonged infusions of the putative differentiating agent sodium phenylbutyrate on myelodysplastic syndromes and acute myeloid leukemia. Clin Cancer Res 2002;8:963–70.
6. Gore SD, Weng LJ, Zhai S, et al. Impact of the putative differentiating agent sodium phenylbutyrate on myelodysplastic syndromes and acute myeloid leukemia. Clin Cancer Res 2001;7:2330–9.
7. Minucci S, Pelicci PG. Histone deacetylase inhibitors and the promise of epigenetic (and more) treatments for cancer. Nat Rev Cancer 2006;6:38–51.
8. Rasheed WK, Johnstone RW, Prince HM. Histone deacetylase inhibitors in cancer therapy. Expert Opin Investig Drugs 2007;16:659–78.
9. Fakih MG, Pendyala L, Fetterly G, et al. A phase I, pharmacokinetic and pharmacodynamic study on vorinostat in combination with 5-fluorouracil, leucovorin, and oxaliplatin in patients with refractory colorectal cancer. Clin Cancer Res 2009;15:3189–95.
10. Ramalingam SS, Parise RA, Ramanathan RK, et al. Phase I study of vorinostat, a histone deacetylase (HDAC) inhibitor, in combination with carboplatin (Cb) and paclitaxel (P) for patients with advanced solid malignancies. Clin Cancer Res 2007;13:3605–10.
11. Bug G, Ritter M, Wassmann B, et al. Clinical trial of valproic acid and all-trans retinoic acid in patients with poor-risk acute myeloid leukemia. Cancer 2005;104:2717–25.
12. Catley L, Weisberg E, Kiziltepe T, et al. Aggresome induction by proteasome inhibitor bortezomib and α-tubulin hyperacetylation by

tubulin deacetylase (TDAC) inhibitor LBH589 are synergistic in myeloma cells. Blood 2006;108:3441–9.
13. Fiskus W, Pranpat M, Bali P, et al. Combined effects of novel tyrosine kinase inhibitor AMN107 and histone deacetylase inhibitor LBH589 against Bcr-Abl-expressing human leukemia cells. Blood 2006;108: 645–52.
14. Rahmani M, Yu C, Dai Y, et al. Coadministration of the heat shock protein 90 antagonist 17-allylamino-17-demethoxygeldanamycin with suberoylanilide hydroxamic acid or sodium butyrate synergistically induces apoptosis in human leukemia cells. Cancer Res 2003; 63:8420–7.
15. Bu P, Gao L, Zhuang J, Feng J, Yang D, Yan X. Anti-CD146 monoclonal antibody AA98 inhibits angiogenesis via suppression of nuclear factor-κB activation. Mol Cancer Ther 2006;5:2872–8.
16. Xie S, Luca M, Huang S, et al. Expression of MCAM/MUC18 by human melanoma cells leads to increased tumor growth and metastasis. Cancer Res 1997;57:2295–303.
17. Ostmeier H, Fuchs B, Otto F, et al. Prognostic immunohistochemical markers of primary human melanomas. Br J Dermatol 2001; 145:203–9.
18. Bots M, Johnstone RW. Rational combinations using HDAC inhibitors. Clin Cancer Res 2009;15:3970–7.
19. Wu GJ, Wu MW, Wang SW, et al. Isolation and characterization of the major form of human MUC18 cDNA gene and correlation of MUC18 over-expression in prostate cancer cell lines and tissues with malignant progression. Gene 2001;279:17–31.
20. Wu GJ, Varma VA, Wu MW, et al. Expression of a human cell adhesion molecule, MUC18, in prostate cancer cell lines and tissues. Prostate 2001;48:305–15.
21. Lai K, Sharma V, Jager MJ, Conway RM, Madigan MC. Expression and distribution of MUC18 in human uveal melanoma. Virchows Arch 2007;451:967–76.
22. Zabouo G, Imbert A-M, Jacquemier J, et al. CD146 expression is associated with a poor prognosis in human breast tumors and with enhanced motility in breast cancer cell lines. Breast Cancer Res 2009;11:R1.
23. Leslie MC, Zhao YJ, Lachman LB, Hwu P, Wu GJ, Bar-Eli M. Immunization against MUC18/MCAM, a novel antigen that drives melanoma invasion and metastasis. Gene Ther 2007;14:316–23.
24. Yan X, Lin Y, Yang D, et al. A novel anti-CD146 monoclonal antibody, AA98, inhibits angiogenesis and tumor growth. Blood 2003; 102:184–91.
25. Xing H, Weng D, Chen G, et al. Activation of fibronectin/PI-3K/Akt2 leads to chemoresistance to docetaxel by regulating survivin protein expression in ovarian and breast cancer cells. Cancer Lett 2008;261: 108–19.
26. Wong YF, Cheung TH, Lo KWK, et al. Identification of molecular markers and signaling pathway in endometrial cancer in Hong Kong Chinese women by genome-wide gene expression profiling. Oncogene 2007;26:1971–82.
27. Wu P, Tian Y, Chen G, et al. Ubiquitin B: an essential mediator of trichostatin A-induced tumor-selective killing in human cancer cells. Cell Death Differ 2010;17:109–18.
28. Zhou J, Gao Q, Chen G, et al. Novel oncolytic adenovirus selectively targets tumor-associated polo-like kinase 1 and tumor cell viability. Clin Cancer Res 2005;11:8431–40.
29. Muthukkaruppan V, Auerbach R. Angiogenesis in the mouse cornea. Science 1979;205:1416–8.
30. Kelly WK, O'Connor OA, Krug LM, et al. Phase I study of an oral histone deacetylase inhibitor, suberoylanilide hydroxamic acid, in patients with advanced cancer. J Clin Oncol 2005;23:3923–31.
31. Satyamoorthy K, Muyrers J, Meier F, Patel D, Herlyn M. Mel-CAM-specific genetic suppressor elements inhibit melanoma growth and invasion through loss of gap junctional communication. Oncogene 2001;20:4676–84.
32. Mills L, Tellez C, Huang S, et al. Fully human antibodies to MCAM/MUC18 inhibit tumor growth and metastasis of human melanoma. Cancer Res 2002;62:5106–14.
33. Li G, Kalabis J, Xu X, et al. Reciprocal regulation of MelCAM and AKT in human melanoma. Oncogene 2003;22:6891–9.
34. Cooper AL, Greenberg VL, Lancaster PS. *In vitro* and *in vivo* histone deacetylase inhibitor therapy with suberoylanilide hydroxamic acid (SAHA) and paclitaxel in ovarian cancer. Gynecol Oncol 2007;104: 596–601.
35. Butler LM, Agus DB, Scher HI, et al. Suberoylanilide hydroxamic acid, an inhibitor of histone deacetylase, suppresses the growth of prostate cancer cells *in vitro* and *in vivo*. Cancer Res 2000;60: 5165–70.
36. Xu Q, Simpson SE, Scialla TJ, Bagg A, Carroll M. Survival of acute myeloid leukemia cells requires PI3 kinase activation. Blood 2003; 102:972–80.
37. Liang D, Kong X, Sang N. Effects of histone deacetylase inhibitors on HIF-1. Cell Cycle 2006;5:2430–5.
38. Deroanne CF, Bonjean K, Servotte S, et al. Histone deacetylases inhibitors as anti-angiogenic agents altering vascular endothelial growth factor signaling. Oncogene 2002;21:427–36.
39. Rogers MS, Birsner AE, D'Amato RJ. The mouse cornea micropocket angiogenesis assay. Nat Protoc 2007;2:2545–50.
40. Kenyon BM, Voest EE, Chen CC, Flynn E, Folkman J, D'Amato RJ. A model of angiogenesis in the mouse cornea. Invest Ophthalmol Vis Sci 1996;37:1625–32.
41. Maeda T, Towatari M, Kosugi H, Saito H. Up-regulation of costimulatory/adhesion molecules by histone deacetylase inhibitors in acute myeloid leukemia cells. Blood 2000;96:3847–56.